RSC Advances

PAPER

View Article Online
View Journal | View Issue

Cite this: *RSC Adv.*, 2019, **9**, 41209

In situ synthesis of ZnO–GO/CGH composites for visible light photocatalytic degradation of methylene blue†

Xiaoxuan Di, Feng Guo,* Zihan Zhu, Zhonghao Xu, Ziqi Qian and Qian Zhang

Received 8th November 2019
Accepted 9th December 2019

DOI: 10.1039/c9ra09260a

rsc.li/rsc-advances

A novel ZnO–GO/CGH composite was prepared using an *in situ* synthesis process for photodegradation of methylene blue under visible light illumination. The chitin–graphene composite hydrogel (CGH) was used to provide uniform binding of the nano ZnO–GO composite to the hydrogel surface and prevent their agglomeration. GO provides multi-dimensional protons and electron transport channels for ZnO with a flower-like structure, which possessed improved photo-catalytic activity. SEM analysis indicates that the hydrogel has good adsorption properties with rougher surfaces and porous microstructure, which enables it to adsorb the dyes effectively. Under synergetic enhancement of adsorption and photo-catalysis, catalytic activity and nano ZnO–GO/CGH recycling improved greatly. Synthesized nano ZnO–GO/CGH showed high dye removal efficiency of 99%, about 2.2 times that of the pure chitin gel under the same condition. This suggests the potential application of the new photocatalytic composites to remove organic dyes from wastewater.

Introduction

Dyes have a wide range of industrial applications including textiles, paper, plastics, printing, cosmetics, and food processing, which result in critical water pollution issues.[1] Accumulation of dyes in water causes mutagenesis and carcinogenesis of aquatic organisms and humans.[2] Organic dyes have received more concern for their potential to cause serious environmental pollution because they are highly toxic and difficult to biodegrade. Methylene blue (MB), a widely used cationic dye, shows thermal and light stability and low biodegradability because of its aromatic ring with a large molecular diameter and large molecular bond energy.[3] Conventional methods of removing dyes, including electrocoagulation–flotation,[4] ion exchange,[5] membrane separation,[6] electrochemistry,[7] oxidation[8] and advanced oxidation,[9] have not achieved the desired results. It is worth noting that adsorption and photocatalysis are the most economical techniques for removing MB.[10,11]

The adsorption process has great potential in the purification of industrial dye wastewater because of its simplicity, cost-effectiveness and low energy consumption. The selection of suitable adsorbents is a key point in industrial applications. The adsorption efficiency of conventional adsorbent materials such as activated carbon, alumina, zeolite, activated and silica gel relies mainly on the adsorption sites in the pores between the layers.[12–15] Different kinds of novel and non-conventional adsorbents with high adsorption capability are constantly emerging. One of those is hydrogels, which possess unique advantages of large surface area, good mechanical/chemical stability and plenty of surface functional groups.[16] These can combine with the dye molecules by forming hydrogen bonds or electrostatic interactions.

It is feasible that hydrogels synthesize by selecting and recognizing substrates by modifying their architecture based on the molecular structure characteristics of dye molecules. According to their starting materials, hydrogels can be divided into natural and synthetic varieties; corresponding representatives are chitin gel (CH) and graphene hydrogels (GH), respectively.[17] GH, a three-dimensional (3D) nanocarbon material derived from graphene oxide (GO), provides high electron mobility, multi-dimensional mass transfer channels and enables efficient absorption of dyes combined with high surface area, special pore structure and plane adsorption properties.[18] However, dyes are not completely purified but only absorbed. Hydrogels with absorbed dyes still have great potential harm to the surroundings and should be treated before discarding. Therefore, they should be combined with chemical degradation to achieve a brighter application foreground in waste-water treatment engineering.

In recent years, the photocatalytic method has become favored, reflecting its superiority in waste-water treatment because of its high efficiency and low energy consumption.[19] TiO_2 is the most researched and applied semiconductor photocatalyst. Unfortunately, it can only absorb ultraviolet rays

Key Laboratory of Industrial Ecology and Environmental Engineering (Ministry of Education), School of Ocean Science and Technology, Dalian University of Technology, Panjin 124221, China. E-mail: 0411guofeng@dlut.edu.cn

† Electronic supplementary information (ESI) available. See DOI: 10.1039/c9ra09260a

beyond the wavelength of 388 nm. ZnO is a suitable alternative to TiO_2 and has a forbidden bandwidth of 3.37 eV.[20] However, the harvest of visible light remains low and the electron–hole recombination ratio is high. Various strategies have been adopted to restrain the combination speed of photogenerated electron–hole pairs.[21–23] This can be achieved by modifying the electronic bandgap structure of ZnO with GO to enhance interfacial charge carrier transfer.[24,25] However, this raises the question of whether GO has its agglomeration and surface poisoning defects. Additionally, the high cost of GO has severely hindered its use. The most recent research indicates that incorporating hydrogels in GO sheets *via* cross-linking agents helps prevent GO layer aggregation, which enables a highly porous three-dimensional structure.[26] Therefore, a ZnO–GO nanocomposite combined with hydrogel will contribute to the perfect combination of adsorption and photo-catalysis.

In this work, we report a simple approach to synthesize a ZnO–GO coupled eco-friendly chitin graphene hydrogel as an efficient visible-light photo-catalyst for MB degradation. The crystal structures, morphology and optical properties of ZnO–GO/CGH composites were analyzed by using SEM images, transmission electron microscopy, X-ray diffraction, FTIR spectroscopy and UV-Vis DRS. The catalytic activity and recycling of ZnO–GO/CGH composites were studied in detail. The relationships among the composites constituents and the photocatalytic activities are discussed. The kinetics mechanisms of adsorption were further studied. ZnO–GO/CGH exhibits a large surface area and interconnected pores in a three-dimensional hydrogel structure, which provides rich active sites for adsorbing MB.

Results and discussion

Structural and morphology analysis of ZnO–GO/CGH

The synthesis of ZnO–GO/CGH is illustrated in Scheme S1.† The morphology and structural characteristics of ZnO, GO, ZnO–GO, CGH and ZnO–GO/CGH samples were observed using FE-SEM and TEM. Fig. 1(a–e) shows FE-SEM images of sheet nano ZnO crystal, GO film, ZnO–GO composite, chitin–GO hydrogel (CGH) and ZnO–GO/CGH composite, respectively. The cross-sectional sizes of ZnO sheet were about 30–45 nm. Fig. 1(c) shows that ZnO nano-sheets were dispersed uniformly on the GO surface. Because chitin does not dissolve but suspends in aqueous alkali, the three-dimensional web-like structure with smooth edges [Fig. 1(d)] is well preserved in CGH after the freezing and thawing treatment. After adding ZnO–GO, the pore structure was obviously retained and the ZnO–GO adhered to the wall [Fig. 1(e and f)]. The retained pore walls are beneficial for improving the adsorption capacity of composite materials. Fig. 1(g and h) reveals that the average length of the surficial ZnO is *ca.* 15 nm and the lattice distance is approximately 0.25 nm. Therefore, the introduction of a GO film decreases the size of nano ZnO but does not affect the morphology of the ZnO nano-sheets. The EDS of ZnO–GO/CGH samples further support the TEM results.

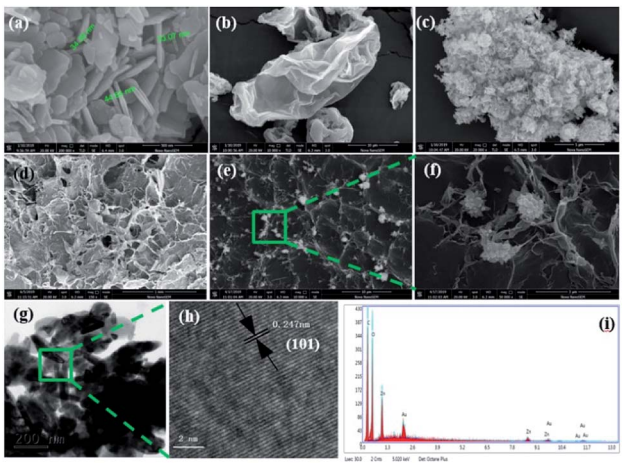

Fig. 1 SEM images of (a) ZnO sheets, (b) GO film, (c) ZnO–GO composite, (d) CGH and (e and f) ZnO–GO/CGH composite. HR-TEM images of (g and h) ZnO–GO/CGH composite and its EDS (i).

The XRD patterns of pure nano ZnO, GO, ZnO–GO, CGH and ZnO–GO/CGH composites are shown in Fig. 2(a). All the major diffraction patterns that correspond to ZnO, ZnO–GO and ZnO–GO/CGH composites are clearly observed at $2\theta = 31.8°$, 34.4°, 36.3°, 47.5°, 56.6°, 62.9°, 66.4°, 67.9°, 69.1°, 72.6° and 76.9°, corresponding respectively to (100), (002), (101), (102), (110), (103), (200), (112), (201), (004) and (202) crystalline planes of ZnO.[28] These peaks are indexed to the hexagonal phase wurtzite structure of ZnO (JCPDS card no. 36-1451 data).[29] The characteristic peaks located at 9.8° corresponding to the (001) crystalline reference plane of GO.[30] The XRD pattern of CGH and ZnO–GO/CGH composites indicates intense diffraction peaks at $2\theta = 20.5°$ and 21.7°, respectively, which are attributed to the amorphous structure of chitin.[31] This further illustrates that the crystal plane of nano ZnO remains complete after being composited with GO and CGH.

Raman spectroscopy is a popular method to identify the defects of carbon-based materials. The Raman spectra of GO, ZnO–GO, CGH and ZnO–GO/CGH exhibited characteristic peaks at about 1325 and 1593 cm^{-1} (Fig. 2(b)), which could be attributed to the significant D and G graphene bands. The D band and G band were related to the defect site of the C atom lattice (disordered sp^3 carbon atoms) and order sp^2 carbon atoms caused by hybridization, respectively.[32] The I_D/I_G values of GO, ZnO–GO, CGH and ZnO–GO/CGH were 1.05, 1.23, 1.20 and 1.15, respectively. GO likely decreased in a complex process involving GO and ZnO or GH. Meanwhile, the defects increases as the disorder degree increases.[33] Moreover, the I_D/I_G value of ZnO–GO was highest among the four composite materials, which indicated that more defects and edges were formed in ZnO–GO. A new 2D band appeared in ZnO–GO after ZnO was introduced to GO, which was attributed to a two-phonon resonance phenomenon.[34] All of this shows that these defects are produced by the oxidation of carbon atoms during the ZnO–GO synthesis process.[35] Furthermore, the Raman spectrum of ZnO–GO/CGH had a slight blue shift compared with that of GO, which indicates that a surficial hybridization reaction occurred.

Fig. 2(c) shows the FTIR spectra of GO, ZnO–GO, CGH, ZnO–GO/CGH and recycled ZnO–GO/CGH. For GO, the peaks at 887,

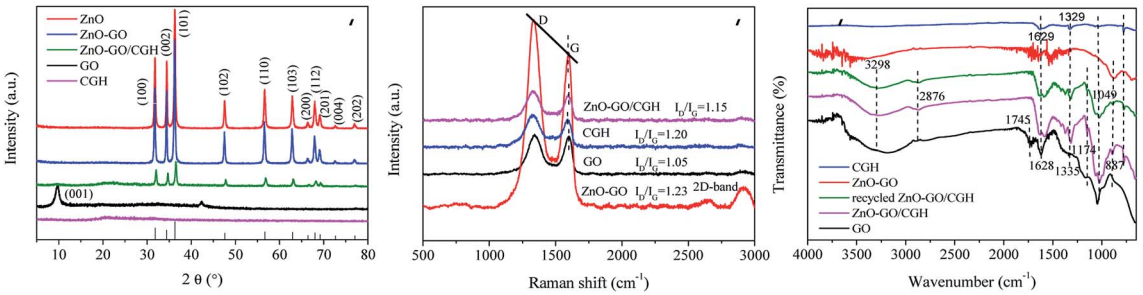

Fig. 2 (a) XRD patterns of GO, ZnO, ZnO–GO, CGH and ZnO–GO/CGH composites. (b) Raman spectra of the GO, ZnO–GO, CGH and ZnO–GO/CGH composites. (c) FTIR spectra of GO, ZnO–GO, CGH, ZnO–GO/CGH and recycled ZnO–GO/CGH composites.

1049, 1628, 1745 and 3298 cm^{-1} correspond to the stretching vibration of C=O, alkoxy C–O, aromatic C=C, sharp C=O and OH bonds, respectively.[36] Compared with GO, the FTIR spectra of ZnO–GO, CGH, ZnO–GO/CGH and recycled ZnO–GO/CGH exhibited weak peaks at 1049 cm^{-1} and 1745 cm^{-1}, which corresponded to the adsorption peaks of the CO stretching vibration. This confirmed the reduction of GO by vitamin C.[37] The respective shifts of peaks from 1629 and 1329 cm^{-1} to 1582 and 1317 cm^{-1} demonstrated the successful introduction of CGH to the ZnO–GO/CGH.[38] The FTIR spectra also confirmed that ZnO–GO/CGH had some oxygen-containing functional groups and defect sites due to the synergistic effect between GO and ZnO.

The reduction of GO was further investigated using XPS spectra of C elements present in GO, CGH and ZnO–GO/CGH samples (Fig. 3). The peaks at the binding energies of 285.2 eV, 532.6 eV, 1021.3 eV and 1044.8 eV corresponded to the C (1s), O (1s), Zn ($2p_{3/2}$) and Zn ($2p_{1/2}$) levels, respectively. The intensity of the C (1s) peaks at 284.6 eV, 285.2 eV and 286.2 eV in GO [Fig. 3(b)] corresponding to the C–C, C–O and C=O, respectively, are stronger than those of ZnO–GO/CGH [Fig. 3(c)], which indicates that part of GO was reduced after the complex reaction.[39] Additionally, the retained oxygen-containing functional groups give ZnO–GO/CGH similar properties to hydrogels in adsorbing and removing pollutants. Fig. 3(d) and (e) shows the XPS signal for Zn ($2p_{3/2}$) and Zn ($2p_{1/2}$) at the binding energies of 1021.2 eV and 1044.3 eV for the ZnO and 1021.1 eV and 1044.1 eV for the ZnO–GO/CGH composite, respectively.[40] The bindings of Zn^{2+} to oxygen in the ZnO matrix and the +2 oxidation state of Zn in the ZnO were also confirmed by a spin–orbit splitting value of 23 eV.[41] The blue shift (−0.2 eV) and C/O ratio increase (+0.04) indicates that the combination of ZnO and GO can effectively promote photoelectron transition and improve the catalyst's photocatalytic activity.[42]

Charge transport and separation are key factors in the photocatalytic activity of composites.[20] Broadening the light response range of semiconductor photocatalysts allows for more efficient use of the visible light. The UV-Vis diffuse reflectance spectra (UV-Vis DRS) of synthesized ZnO, GO, ZnO–GO, CGH and ZnO–GO/

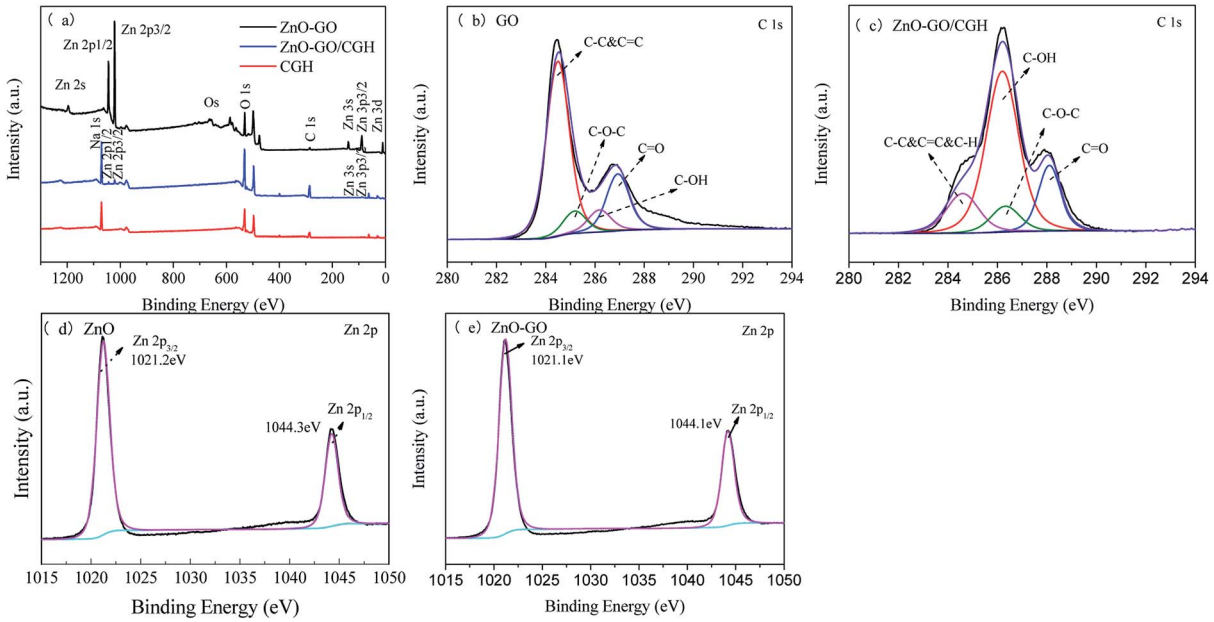

Fig. 3 (a) XPS spectra of ZnO–GO, CGH and ZnO–GO/CGH composites, (b) C 1s region of GO, (c) C 1s region of ZnO–GO/CGH, (d) Zn 2p region of ZnO and (e) Zn 2p region of ZnO–GO.

CGH samples are shown in Fig. 4. All samples have strong absorption peaks at 200–400 nm, which can be related to the band gap absorption of ZnO. ZnO and GO showed the strongest and weakest absorption in visible-light, respectively. The other three composites demonstrated stronger and more stable absorption in the visible region than that of ZnO. Therefore, introducing GO significantly affects the ZnO band gap and the band gap energy of ZnO–GO is smaller than that of pure ZnO.[37] It is noteworthy that ZnO–GO/CGH exhibits very strong absorption in both ultraviolet and visible light. Because enhanced absorption results in more electron–hole pairs and higher photocatalytic activity,[43] this increased absorption improves the photocatalytic activity of ZnO–GO/CGH.

To further explain the photocatalytic mechanism of ZnO–GO composites, the photocurrent response test was performed. As shown in Fig. S1,† the photocurrent intensity of ZnO increase after combining with GO, the photocurrent density of ZnO–GO is almost 3-times higher than that of pure ZnO, indicating the more efficient photoinduced charge separation and transfer over the ZnO–GO composite. N_2 sorption isotherms analysis was used to assess the surface area and the pore volume of ZnO, ZnO–GO, CGH and ZnO–GO/CGH. The adsorption–desorption isotherms are shown in Fig. S2.† The data of Brunauer–Emmett–Teller surface area, pore volume and pore size of samples are listed in Table S1.† All samples exhibit Type III isotherm and H3 hysteresis, which indicates the presence of pores in the sample.[44] The specific surface area in the ZG/CGH hydrogel composite is 18.76 $m^2\ g^{-1}$, which is higher than that of pure CGH (9.952 $m^2\ g^{-1}$). The ZnO–GO has a larger porosity than the GO–ZnO particles, which suggests that the CGH coating decreases the surface area of ZnO and ZnO–GO. Partly as a result, the photocatalytic activity is decreased. However, the three-dimensional CGH network structure with enhanced graphene surface area and interconnected porous channels has the advantages of free separation, high capacity adsorption and photocatalytic reduction to remove MB from aqueous solutions.[45]

TGA curves of GO, ZnO, ZnO–GO, CGH and ZnO–GO/CGH are shown in Fig. S3.† ZnO–GO shows similar thermal stability to ZnO at temperatures above 300 °C with less than 3.8% weight loss, which is attributed to the presence of ZnO in the structure.[46] The residual weights of the neat CGH and ZnO–GO/CGH are 40.1% and 46.2%, respectively. There were mass losses at <110 °C and 150–200 °C, which can be ascribed to the loss of the bound water and side oxygen-containing groups such as acid and ester groups, respectively. The most obvious stage of decomposition is at 230 °C, which is attributed to the degradation of the chitin chains. At temperatures over 450 °C, the main chain of CGH begins to degrade.[47] The incorporation of ZnO–GO into the carrier CGH can improve the thermal stability of CGH. Therefore, the prepared ZnO–GO/CGH had high thermal stability at elevated temperatures because of the interaction between GO and ZnO.

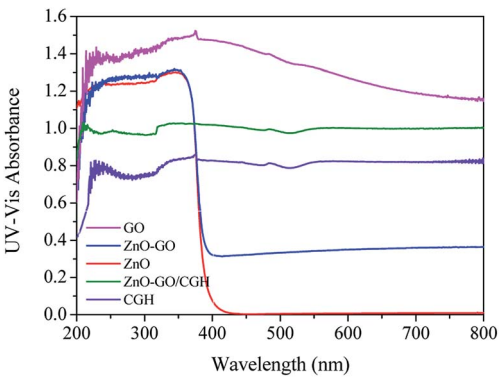

Fig. 4 UV-visible diffuse reflectance spectroscopy (DRS) of GO, ZnO, ZnO–GO, CGH, and ZnO–GO/CGH composites.

Adsorption kinetics

CGH possess abundant hydroxyl groups and pores that can adsorb MB through various interactions. Because of the high cost of photocatalyst systems, it is preferable to screen the optimum ratio of GO/CH in carrier CGH. In this investigation, 1 g L^{-1} of CGH was used for adsorption under dark conditions and methylene blue concentration of 30 mg L^{-1} (Fig. 5(a)). By increasing the GO/CGH ratio to 1/10, the adsorption rate of CGH for MB improved to a relatively high level (73%). A higher GO/CH ratio helps to improve the adsorption rate but also raises the cost of photocatalyst systems. The MB adsorption on CGH reached 73% of equilibrium C/C_0 during the first 30 min of contact, benefiting from the early MB adsorption on the CGH due to the fast diffusion and surface interactions. Therefore, a CGH with GO/CH ratio of 1/10 were used for further dynamic adsorption discussion.

The kinetics of MB adsorption on CGH were analyzed using pseudo-first-order and pseudo-second-order kinetics. The proposed pseudo-first order model (eqn (1)) and pseudo-second order model (eqn (2)) can be represented by the following equations:[48]

$$q_t = q_e(1 - e^{-K_1 t}) \quad (1)$$

$$q_t = \frac{q_e^2 K_2 t}{1 + q_e K_2 t} \quad (2)$$

where q_e and q_t are the amount of absorbed MB at equilibrium (mg g^{-1}). At any time t (mg g^{-1}), K_1 (min^{-1}) and K_2 (g $mg^{-1}\ min^{-1}$) are the equilibrium rate constants for modeling.

The theoretical isotherm parameters, K_1 (min^{-1}), K_2 (g $mg^{-1}\ min^{-1}$), q_e (mg g^{-1}) and the correlation coefficients (R^2) are listed in Table S2.† These two kinetic models are applied for fitting the curves in Fig. 5(b and c). The correlation coefficient R^2 value of 0.999 indicated that the pseudo-second-order kinetic fits properly the MB adsorption on CGH. It is certain that chemisorption might be the rate-limiting step controlling the adsorption process in CGH system and the adsorption rate depends on the sorption capacity rather than the adsorbate concentration.[49,50]

Photocatalytic MB degradation

First of all, to investigate the effect of reduction of GO by vitamin C on its catalytic efficiency, the contrast experiments of photocatalytic performance of ZnO–GO/CGH without VC was

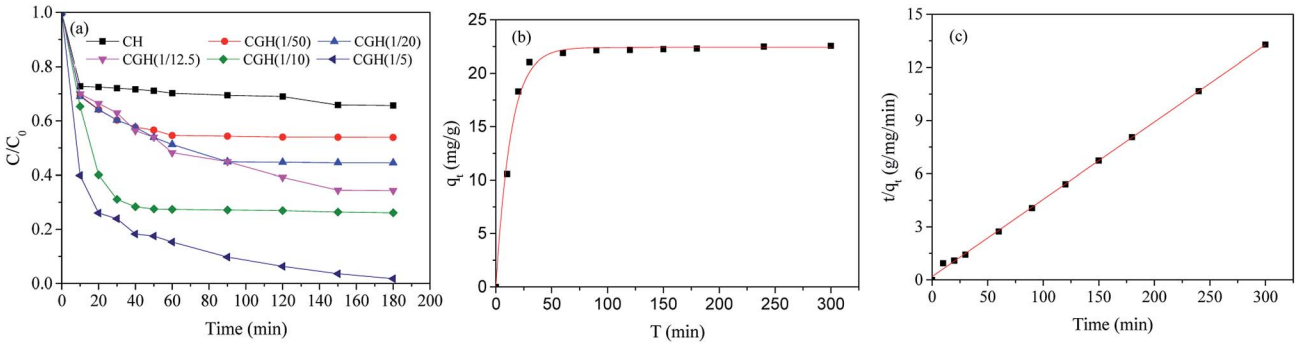

Fig. 5 (a) Adsorption of 30 mg L^{-1} MB on different proportions of chitin graphene hydrogel; kinetics of adsorption of MB by CGH (GO/CGH = 1/10): (b) pseudo first (c) pseudo second-order kinetic diagram; (initial concentration of MB: 30 mg L^{-1}; catalyst dosage: 1.0 g L^{-1}; temperature: 25 °C; pH = 7.0).

also studied (Fig. S4†). After the reduction of GO by VC, the dark adsorption and the final removal efficiency of MB decreased by 43% and 44%, respectively. It is presumed that partial reduction of GO enhanced the hydrophobicity and π–π stacking interactions and thus improved the photocatalytic efficiency.

The loading of ZnO–GO on the degradation process was evaluated by varying the mass ratio of ZnO–GO to CGH. The resultant photocatalytic performance of the ZnO–GO/CGH was tested by MB photodegradation under visible light illumination. Before illumination, ZnO–GO/CGH was added to MB solution and magnetically stirred in the dark for about 30 min to achieve a balance of adsorption and desorption. As shown in Fig. 6(a), the ZnO–GO/CGH exhibited lower MB removal efficiency compared with that of CGH for 60 min. The physical adsorption was likely overwhelmingly superior at this stage. The introduction of ZnO–GO is unfavorable to MB adsorption. With increasing irradiation time, the photocatalyst species played a major role and obtained a higher MB removal efficiency. The proportion of ZnO–GO in ZnO–GO/CGH affected the photo-degradation efficiency. The catalyst with low ZnO–GO content (<1 wt%) exhibited low activity. If the content was high enough, it accumulated at the surface of the pore of CGH, which caused local congestion (Fig. 1(f)). The influences of doping ZnO–GO on the gel strength were also studied. The results obtained were in the range of 1.98–18.80 N (Fig. S5†). The gel strength was obviously affected by ZnO–GO doping, which benefitted the chemical crosslinking network between the CGH and ZnO–GO. However, higher gel strength decreases the water holding capacity of ZnO–GO/CGH, which further affects MB adsorption. The optimum content of ZnO–GO in ZnO–GO/CGH was selected as 1 wt%.

The effect of initial MB concentration (30, 40, 45 and 50 mg L^{-1}) on MB degradation was studied under visible light. Such concentrations could be higher than actual concentrations in contaminated dye wastewater. The amount of degraded contaminant decreased with increasing contaminant concentration in ZnO–GO/CGH catalytic experiments (Fig. 6(b)). MB at 30 mg L^{-1} resulted in a relatively high removal efficiency of 74% after 30 min exposure. The results showed that the remaining contaminant concentration remained high. The effect of catalyst amount on the MB photodegradation rate was further investigated by varying the amount of catalyst used in the range of 0.25–1.25 g L^{-1} keeping MB concentration preset at 30 mg L^{-1} (Fig. 6(c)). The degradation rate initially increased with increasing photocatalyst amount, as the hydroxyl radicals from active sites on the photocatalyst surface increased. When longer times are allowed, lower catalyst amounts are acceptable. We selected 1.0 g L^{-1} catalyst for the following photodegradation process.

The photocatalytic performance of ZnO–GO/CGH with different pH values was studied with initial pH ranging from 3.0 to 11.0 (Fig. 6(d)). With increasing pH value, the degradation efficiency first increased from pH 3.0 to 7.0 and then decreased at pH 9.0. This may be partially because the material surface charge, molecule charge and organic molecule adsorption on the surface of photocatalyst are strongly influenced by pH.[51] Moreover, the initial pH of solution was adjusted by a NaOH or HCl aqueous solution and H^+/Cl^{-1} will affect the photocatalytic activity of the photocatalyst *via* electrostatic interaction of H^+ and competition functions of Cl^{-1}, respectively.[52]

ZnO–GO/CGH recycling

Recycling of 1 wt% ZnO–GO/CGH was investigated in the presence of visible light irradiation. Photodegradation efficiency of the sample showed almost no change during the third recycles (Fig. S6†). After five repetitions, the catalytic activity remained comparable to the new catalytic system with a removal rate of 93%. A 50% degradation decrease was observed after eighth recycling, which indicates that the ZnO–GO/CGH can be well recovered and remain stable for MB removal. Therefore, the ZnO–GO/CGH composite is of great potential as reusable photodegradation catalyst of dyes from wastewater.

Photocatalytic mechanism

Under vis-light irradiation, photogenerated holes (h^+) and electrons (e^-) are produced in the valence (VB) and conduction bands (CB), respectively, in the ZnO loaded on the rGO surface. In the ZnO–GO/CGH system, the photogenerated electrons were taken by the rGO and the photo-generated charge separation efficiency increased. The photogenerated holes and electrons moved to different locations on the

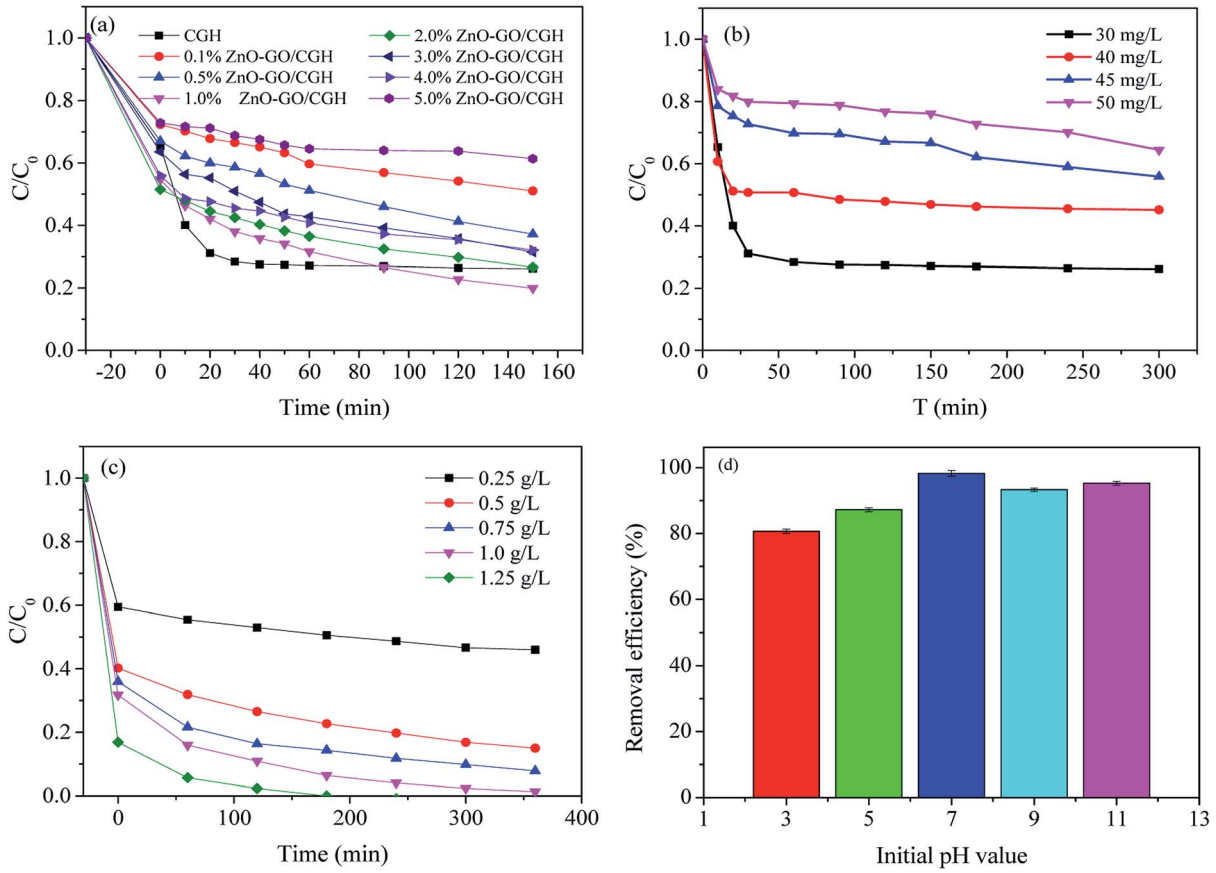

Fig. 6 (a) Photocatalytic activity of different proportions of ZnO–GO/CGH during methylene blue removal (C_0, 30 mg L^{-1}; catalyst dosage, 1.0 g L^{-1}); (b) adsorption experiments of CGH (1/10) on different substrate concentrations (MB); (c) photocatalytic activity of ZnO–GO/CGH having different qualities during MB removal (C_0, 30 mg L^{-1}; catalyst dosage, 1 wt% ZnO–GO/CGH); (d) effect of initial pH.

surface of ZnO–GO/CGH, and formed hydroxyl radical (·OH) and $\cdot O_2^-$, respectively, for MB photodegradation. ·OH, $\cdot O^{2-}$ and h^+ are the uppermost active radical species in the photodegradation process of organic pollutants.[53,54] Reasonable reactions involved in the formation of radicals are presented in eqn (3)–(9).

$$ZnO + h\nu \rightarrow e^- + h^+ \quad (3)$$

$$h^+ + H_2O \rightarrow H^+ + \cdot OH \quad (4)$$

$$e^- + O_2 \rightarrow \cdot O_2^- \quad (5)$$

$$\cdot O_2^- + H^+ \rightarrow HO_2^\cdot \quad (6)$$

$$2HO_2^\cdot \rightarrow H_2O_2 + O_2 \quad (7)$$

$$\cdot OH + MB \rightarrow CO_2 + H_2O \quad (8)$$

$$\cdot O_2^- + e^- + MB \rightarrow CO_2 + H_2O \quad (9)$$

To further confirm the proposed mechanism of ZnO/rGO possessing a high degradation rate, free radical trap experiments were carried out. This could provide information on the capture behavior using EDTA-2Na, isopropanol, $AgNO_3$ and *p*-benzoquinone (*p*-BQ) as holes (h^+), hydroxyl radicals (·OH), electrons (e^-) and superoxide radicals ($\cdot O_2^-$) scavenger.[55,56] The photocatalytic performance of 1 wt% ZnO–GO/CGH was significantly decreased after adding electrons ($AgNO_3$) and superoxide (*p*-BQ) radical scavenger (Fig. S7†), which suggests that ZnO–GO/CGH has a similar degradation mechanism to traditional ZnO (Fig. S8†).

Experimental

Materials

Zinc sulfate heptahydrate ($ZnSO_4 \cdot 7H_2O$, 99.5%), sodium hydroxide (NaOH, 96%), hexamethylenetetramine ($C_6H_{12}N_4$, 99%) and methylene blue (MB, 98%) were purchased from Damao Chemical Reagent Factory (Tianjin, China). Graphene oxide (GO, 99%) was purchased from Suzhou Carbon Technology Co. (Jiangsu, China). Urea (H_2NCONH_2, 99%) was purchased from Sinopharm Chemical Reagent Co., Ltd. (Shanghai, China). Chitin [$(C_8H_{13}NO_5)_n$] was purchased from Aladdin. Ascorbic acid ($C_6H_8O_6$, 99.7%) was purchased from Tianjin Kemiou Chemical Reagent Co., Ltd. (Tianjin, China). All chemicals were analytical reagents and used as received without further purification.

Preparation of the nano ZnO and ZnO–GO composites

Nano ZnO was prepared in a 100 mL Teflon hydrothermal vessel. In a typical process, 20 mL 0.08 g mL^{-1} sodium hydroxide aqueous solution was added dropwise to 30 mL 0.8 g mL^{-1} zinc sulfate heptahydrate in the presence of ultrasonic irradiation, which gave a milky precipitate. After being maintained for 15 min, 0.5 g hexamethylenetetramine was slowly added. The reaction Teflon vessel was then immersed in a thermostat-controlled oil-bath controlled at 90 °C with vigorous magnetic stirring. After 9 h, the mixture was cooled to room temperature, centrifuged and then washed with deionized water. The resulting sample was dried by lyophilization and then used as a catalyst.

Nano ZnO–GO composites with a different weight loading of GO (0.5 wt%, 1 wt%, 2 wt%, 5 wt%, and 10 wt%) were synthesized. First, graphene nanosheets were obtained using ultrasonic peeling. Typically, 3 mg graphite oxide was dispersed in 40 mL deionized water by sonication for 30 min. Subsequently, nano ZnO was added to the graphene nanosheets suspension after stirring. Then the mixture was kept in a Teflon vessel at 90 °C. After magnetic stirring for 9 h, the resulting samples were filtered, washed with deionized water and lyophilized.

Preparation of ZnO–GO/CGH

First, chitin–GO hydrogel was synthesized as described by Song *et al.*[27] In brief, 0.2 g GO was dispersed in 83 mL distilled water in a flask and placed in ultrasonic equipment. During the ultrasonic treatment, 11 g NaOH and 4 g urea were added to the GO suspension. After addition 2 g of chitin, the mixture was treated by ultrasonic vibration for 2 h. By using the freezing (−30 °C) and thawing process, a bright mixing solution was obtained and then centrifuged at 8000 rpm for 15 min. The resulting solution was labeled as CGH and further mixed with ZnO–GO with ultrasound applied. One gram vitamin C was added to the flask and placed in a water bath preset at 95 °C for 2 h. The resulting product ZnO–GO/CGH was washed with deionized water several times and dried by vacuum freeze-drying. The influence factors of the ZnO–GO/CGH ratio ranged between 0.1 wt% and 5.0 wt% and the GO/CH ratio in CGH varied between 1 : 50 and 1 : 5.

Characterization

The microstructure of the catalysts was characterized using a Nova NanoSEM 450 (FEI) field-emission scanning electron microscope (FE-SEM) equipped with an energy dispersive X-ray (EDX) spectrometer operating at an acceleration voltage of 20 kV and working distance of 5 mm. Transmission electron microscopic (TEM) observations were conducted using a Tecnai G2 F30 (FEI, Netherlands) electron microscope operating at an accelerating voltage of 200 kV. Surface functional groups of solid catalysts were characterized using Fourier transform infrared (FT-IR) spectroscopy (ThermoFisher Scientific, USA) using an ATR cell with a scanning range from 500 to 4000 cm^{-1}. The catalysts' crystal structure was analyzed using X-ray diffraction (XRD; XRD-7000s, Shimadzu, Japan), measured with CuKα (λ = 0.154 nm) radiation at 40 kV and 20 mA by scanning at a rate of 5° min^{-1} in the 2θ range of 1–90°. Specific surface areas were determined by N_2 adsorption at 77 K with the Brunauer–Emmett–Teller method using an Autosorb-iQ-C chemisorption analyzer (Quantachrome Instruments, USA). Thermo-gravimetric analysis (TGA) was conducted using a TGA/DSC1 (METTLER-TOLEDO, Switzerland) at a nitrogen heating rate of 10 °C min^{-1} over a temperature range of 30 °C to 800 °C. X-ray photoelectron spectroscopy (XPS; ESCALAB™ 250Xi) was performed using non-monochromatic Al Kα radiation X-rays to investigate the chemical states of the photocatalysts. Ultraviolet-visible (UV-Vis) diffuse reflectance spectra of ZnO–GO/CGH were measured on an ultraviolet-visible diffuse reflectometer (UV-Vis DRS; LAMBDA 950) with a scan range of 200–800 nm and by using $BaSO_4$ as a reference material. A Raman spectrometer, Renishaw inVia, was used to further confirm the crystal phases of the ZnO–GO. The samples were exposed for 4 s during excitation using the 632.8 nm Ar^+ line. Photoelectrochemical characterization was performed in the three-electrode cell. The light source consists of a 50 W Xe lamp with a cut off filter 420 nm. The samples were coated on a 2 cm × 2 cm stainless steel wire mesh as the working electrode. Ag/AgCl, saturated calomel electrode, and 0.5 M Na_2SO_4 were used as the counter electrode, reference electrode, and electrolyte, respectively.

Static system reaction-synergy of adsorption and photocatalysis in removing MB

The photocatalytic experiments for methylene blue (MB) degradation were conducted in a quartz glass reactor. The contents are exposed to a xenon lamp with a power of 300 W. The solution in the reactor is stirred by agitating magnetically and maintaining a constant temperature of 25 ± 2 °C by circulating water. In a typical process, 0.1 g of each photocatalyst was dispersed in 100 mL MB solution and magnetically stirred in the dark plant for about 30 min to achieve a balance of adsorption and desorption. The photo-degradation reactions were then performed under the radiation of xenon lamp (light source controller, λ = 420 nm) with stirring speed 200 rpm. All experiments were done in triplicate.

The sample analysis was done by UV-5200 UV-Vis spectrophotometer. MB degradation rate (R) can be calculated by eqn (10):

$$R = \left(1 - \frac{C_t}{C_0}\right) \times 100\% \quad (10)$$

where C_0 and C_t are the initial and final concentrations of MB at different time intervals, respectively.

Conclusions

A novel chitin graphene hydrogel supported ZnO–GO with a three-dimensional (3D) network structure was fabricated by a simple hydrothermal method. SEM images show that nano-ZnO sheets were dispersed uniformly on the GO surface. The crystalline wurtzite-like structure of ZnO and ZnO–GO

compounds has been verified by XRD. The XPS spectra indicate that the ZnO–GO combination can effectively promote photoelectron transition and improve the catalyst's photocatalytic activity. During ZnO–GO/CGH synthesis, a surficial hybridization reaction occurred and GO decreased to rGO. MB photodegradation from water under visible light was investigated; MB's photocatalytic performance of 99% was obtained after 150 min. ZnO–GO/CGH catalysts revealed generally similar photocatalytic performance compared with bare ZnO and ZnO–GO catalyst. According to the results from trapping experiments, photogenerated holes and $\cdot O_2^-$ radicals were the main active species in the MB photodegradation process. The stability and reuse of the ZnO–GO/CGH photocatalytic composites confirms their promising potential for advanced wastewater treatment.

Conflicts of interest

There are no conflicts to declare.

Acknowledgements

The authors wish to acknowledge the financial support from China National Natural Science Foundation (No. 31270620), Fundamental Research Funds for the Central Universities (No. DUT19JC13) and Dalian Scientific and Technological Innovation Foundation (No. 2018J12SN072).

Notes and references

1 C. Li, H. Liao, X. Zhang, X. Yu and M. Tong, *J. Appl. Polym. Sci.*, 2017, **134**, 45363.
2 T. Dou, L. Zang, Y. Zhang, Z. Sun, L. Sun and C. Wang, *Mater. Lett.*, 2019, **244**, 151–154.
3 R. Kannaujia, V. Prasad, Sapna, P. Rawat, V. Rawat, A. Thakur, S. Majumdar, M. Verma, G. K. Rao, A. P. Gupta, H. Kumar and C. M. Srivastava, *Mater. Lett.*, 2019, **252**, 198–201.
4 N. Nippatla and L. Philip, *Process Saf. Environ. Prot.*, 2019, **125**, 143–156.
5 J. Pan, D. Zhang, M.-M. Shang, Y. Mu, S.-D. Han and G.-M. Wang, *J. Lumin.*, 2019, **210**, 70–74.
6 J. Saikia, S. Sarmah, J. J. Bora, B. Das and R. L. Goswamee, *Bull. Mater. Sci.*, 2019, **42**, 104.
7 C. N. Brito, M. B. Ferreira, E. C. M. de Moura Santos, J. J. L. Léon, S. O. Ganiyu and C. A. Martínez-Huitle, *J. Appl. Electrochem.*, 2018, **48**, 1321–1330.
8 L. Wolski, A. Walkowiak and M. Ziolek, *Catal. Today*, 2019, **333**, 54–62.
9 C. Yang, X. Kong, L. Zhu and D. Wang, *Desalin. Water Treat.*, 2018, **132**, 307–316.
10 T. Hertel, R. M. Novais, R. Murillo Alarcón, J. A. Labrincha and Y. Pontikes, *J. Cleaner Prod.*, 2019, **227**, 877–889.
11 G. Liao, J. Fang, Q. Li, S. Li, Z. Xu and B. Fang, *Nanoscale*, 2019, **11**, 7062–7096.
12 W. Astuti, T. Sulistyaningsih, E. Kusumastuti, G. Thomas and R. Y. Kusnadi, *Bioresour. Technol.*, 2019, **287**, 121426.
13 A. Teimouri, N. Ghased, S. G. Nasab and S. Habibollahi, *Desalin. Water Treat.*, 2019, **139**, 327–341.
14 Z. Majid, A. A. AbdulRazak and W. A. H. Noori, *Arabian J. Sci. Eng.*, 2019, **44**, 5457–5474.
15 A. Salama, H. A. Aljohani and K. R. Shoueir, *Mater. Lett.*, 2018, **230**, 293–296.
16 Y. Li, W. Cui, L. Liu, R. Zong, W. Yao, Y. Liang and Y. Zhu, *Appl. Catal., B*, 2016, **199**, 412–423.
17 C. Liu, H. Liu, T. Xiong, A. Xu, B. Pan and K. Tang, *Polymers*, 2018, **10**, 835.
18 K. C. Wasalathilake, D. G. D. Galpaya, G. A. Ayoko and C. Yan, *Carbon*, 2018, **137**, 282–290.
19 W. Zhong, S. Shen, S. Feng, Z. Lin, Z. Wang and B. Fang, *CrystEngComm*, 2018, **20**, 7851–7856.
20 D. Zhang, Y. Zhao and L. Chen, *Appl. Surf. Sci.*, 2018, **458**, 638–647.
21 W. Zhong, S. Shen, M. He, D. Wang, Z. Wang, Z. Lin, W. Tu and J. Yu, *Appl. Catal., B*, 2019, **258**, 117967.
22 W. Zhong, W. Tu, S. Feng and A. Xu, *J. Alloys Compd.*, 2019, **772**, 669–674.
23 W. Zhong, Z. Lin, S. Feng, D. Wang, S. Shen, Q. Zhang, L. Gu, Z. Wang and B. Fang, *Nanoscale*, 2019, **11**, 4407–4413.
24 S. P. Lonkar, V. Pillai and A. Abdala, *Appl. Surf. Sci.*, 2019, **465**, 1107–1113.
25 L. Wang, Z. Li, J. Chen, Y. Huang, H. Zhang and H. Qiu, *Environ. Pollut.*, 2019, **249**, 801–811.
26 S. Wang, J. Feng, Q. Meng, B. Cao and G. Tian, *J. Solid State Electrochem.*, 2019, **23**, 2377–2390.
27 X. Song, S. Cui, Z. Li, Y. Jiao and C. Zhou, *J. Mater. Sci.: Mater. Med.*, 2018, **29**, 108.
28 H. Jiang, X. Zhang, W. Gu, X. Feng, L. Zhang and Y. Weng, *Chem. Phys. Lett.*, 2018, **711**, 100–106.
29 A. Shanmugasundaram, R. Boppella, Y.-J. Jeong, J. Park, Y.-B. Kim, B. Choi, S. H. Park, S. Jung and D.-W. Lee, *Mater. Chem. Phys.*, 2018, **218**, 218–228.
30 S. Kumar, A. Garg, A. Chowdhuri, A. Jain and A. Kapoor, *Mater. Res. Express*, 2019, **6**, 075039.
31 C. Qi, L. Zhao, Y. Lin and D. Wu, *J. Colloid Interface Sci.*, 2018, **517**, 18–27.
32 S. Yang, X. Guo, P. Chen, D.-w. Xu, H.-f. Qiu and X.-y. Zhu, *J. Alloys Compd.*, 2019, **797**, 1310–1319.
33 B. Xue and Y. Zou, *J. Colloid Interface Sci.*, 2018, **529**, 306–313.
34 P. Kumbhakar, A. Pramanik, S. Biswas, A. K. Kole, R. Sarkar and P. Kumbhakar, *J. Hazard. Mater.*, 2018, **360**, 193–203.
35 M. Azarang, M. Sookhakian, M. Aliahmad, M. Dorraj, W. J. Basirun, B. T. Goh and Y. Alias, *Int. J. Hydrogen Energy*, 2018, **43**, 14905–14914.
36 A. J. Jafari, R. R. Kalantary, A. Esrafili and H. Arfaeinia, *Process Saf. Environ. Prot.*, 2018, **116**, 377–387.
37 Y. Zhang, W. Cui, W. An, L. Liu, Y. Liang and Y. Zhu, *Appl. Catal., B*, 2018, **221**, 36–46.
38 J. A. Gonzalez, J. G. Bafico, M. E. Villanueva, S. A. Giorgieri and G. J. Copello, *Carbohydr. Polym.*, 2018, **188**, 213–220.
39 C. Liu, M. Yue, L. Liu, Y. Rui and W. Cui, *RSC Adv.*, 2018, **8**, 22402–22410.

40 A. Hui, J. Ma, J. Liu, Y. Bao and J. Zhang, *J. Alloys Compd.*, 2017, **696**, 639–647.
41 S. Meti, M. R. Rahman, M. I. Ahmad and K. U. Bhat, *Appl. Surf. Sci.*, 2018, **451**, 67–75.
42 V. H. Luan, H. N. Tien and S. H. Hur, *J. Colloid Interface Sci.*, 2015, **437**, 181–186.
43 R. Beura and P. Thangadurai, *J. Environ. Chem. Eng.*, 2018, **6**, 5087–5100.
44 Y. Shen, S. Luo, Z. Wu, M. Cao, F. Gu and L. Wang, *J. Mater. Sci.: Mater. Electron.*, 2016, **27**, 12660–12668.
45 Y. Zhao, X. Liu, M. Qi, T. Bai, K. Zhao and X. Zhang, *Coatings*, 2019, **9**, 218.
46 G. Ahmed, M. Hanif, A. J. Khan, L. Zhao, J. Zhang and Z. Liu, *Mater. Chem. Phys.*, 2018, **212**, 479–489.
47 I. Corazzari, R. Nisticò, F. Turci, M. G. Faga, F. Franzoso, S. Tabasso and G. Magnacca, *Polym. Degrad. Stab.*, 2015, **112**, 1–9.
48 M. Ahmad, K. Manzoor, P. Venkatachalam and S. Ikram, *Int. J. Biol. Macromol.*, 2016, **92**, 910–919.
49 B. C. Melo, F. A. A. Paulino, V. A. Cardoso, A. G. B. Pereira, A. R. Fajardo and F. H. A. Rodrigues, *Carbohydr. Polym.*, 2018, **181**, 358–367.
50 S. S. Mayakaduwa, P. Kumarathilaka, I. Herath, M. Ahmad, M. Al-Wabel, Y. S. Ok, A. Usman, A. Abduljabbar and M. Vithanage, *Chemosphere*, 2016, **144**, 2516–2521.
51 H.-Y. Wu, W.-J. Jian, H.-F. Dang, X.-F. Zhao, L.-Z. Zhang and J.-H. Li, *Pol. J. Environ. Stud.*, 2017, **26**, 871–880.
52 N. I. Md Rosli, S.-M. Lam, J.-C. Sin, I. Satoshi and A. R. Mohamed, *J. Environ. Eng.*, 2018, **144**, 04017091.
53 S. Xue, C. Wu, S. Pu, Y. Hou, T. Tong, G. Yang, Z. Qin, Z. Wang and J. Bao, *Environ. Pollut.*, 2019, **250**, 338–345.
54 A. Samadi-Maybodi and M.-R. Sadeghi-Maleki, *J. Inorg. Organomet. Polym. Mater.*, 2018, **28**, 2620–2632.
55 H. Y. Ma, L. Zhao, L. H. Guo, H. Zhang, F. J. Chen and W. C. Yu, *J. Hazard. Mater.*, 2019, **369**, 719–726.
56 F. Chen, W. An, L. Liu, Y. Liang and W. Cui, *Appl. Catal., B*, 2017, **217**, 65–80.